Response of biological productivity to North Atlantic marine front migration during the Holocene

David J. Harning[1,2], Anne E. Jennings[2], Denizcan Köseoğlu[3], Simon T. Belt[3], Áslaug Geirsdóttir[1], Julio Sepúlveda[2]

5 [1]Faculty of Earth Sciences, University of Iceland, Reykjavík, Iceland
[2]Institute of Arctic and Alpine Research, University of Colorado and Department of Geological Sciences, University of Colorado, Boulder, USA
[3]Biogeochemistry Research Centre, Plymouth University, Plymouth, UK

Correspondence to: David J. Harning (david.harning@colorado.edu)

10   **Abstract.** Marine fronts delineate the boundary between distinct water masses and, through the advection of nutrients, are important facilitators of regional productivity and biodiversity. As the modern climate continues to change the migration frontal zones is evident, but a lack of information about their status prior to instrumental records hinders future projections. Here, we combine data from lipid biomarkers (archaeal isoprenoid glycerol dibiphytanyl glycerol tetraethers and algal highly branched isoprenoids) with planktic and benthic foraminifera assemblage to detail the biological response of the marine Arctic

15   and Polar Front migrations on the North Iceland Shelf (NIS) over the last 8 ka. This multi-proxy approach enables us to quantify the thermal structure relating to Arctic and Polar Front migration, and test how this influences the corresponding changes in local pelagic productivity. Our data show that following an interval of Atlantic Water influence, the Arctic Front and its associated high pelagic productivity stabilized on the NIS at ~6.1 ka BP. Following a subsequent trend of regional cooling, Polar Water from the East Greenland Current and the associated Polar Front spread onto the NIS by ~3.8 ka BP,

20   greatly diminishing local algal productivity. Within the last century, the Arctic and Polar Fronts have moved back to their current positions relative to the NIS and helped stimulate the productivity that partially supports Iceland's economy. Our Holocene records from the NIS provide important analogues for how the current frontal configuration and the productivity that it supports may change as global temperatures continue to rise.

1 Introduction

Marine fronts separate different water masses and are a globally ubiquitous feature in the oceans (Belkin et al., 2009). By nature, marine fronts are characterized by strong horizontal gradients of typically correlated water properties, such as temperature, salinity and nutrients. Some fronts influence the position of geostrophic currents that act as conduits for heat, salt and nutrient transport (i.e. density front), whereas others contribute to localized hot spots of primary productivity and

30   biodiversity (i.e. convergent front) (Belkin, 2004; Belkin et al., 2009). Moreover, the combination of downwelling with

enhanced productivity at marine fronts can lead to increase sedimentation rates, while interactions between surface waters and the overlying troposphere can generate wind and precipitation anomalies (Minobe et al., 2008; Small et al., 2008; Belkin et al., 2009 and references therein). Hence, marine fronts exert a broad and significant impact on various physical, chemical, and biological aspects of the global climate system. As the state of the density-driven oceanic circulation pattern in our near future
35   remains uncertain (e.g. Rahmstorf et al., 2015), gaining an improved understanding of the dynamic nature of frontal systems over time will allow us to improve forecasts in these sensitive regions.

The marine fronts in the North Atlantic mark the boundary between warm and saline Atlantic Water that advect equatorial heat northward (Buckley and Marshall, 2015) and Polar Water that transports freshwater and drift ice southward from the Arctic Ocean (Fig. 1, Swift and Aagaard, 1981). Today, most of the North Iceland Shelf (NIS) is influenced by Arctic
40   Water that lies between these two endmembers (Fig. 1, Stefánsson, 1962). In the Iceland Sea, Atlantic Water is transformed by winter cooling and mixing with Polar Water to produce dense Arctic water that sinks to intermediate depths and flows into the North Atlantic to form North Atlantic Deep Water (Swift and Aagaard, 1981; Malmberg and Jonsson, 1997). The Arctic Front (AF) separates Arctic and Atlantic Water, whereas the Polar Front (PF) separates the Arctic and Polar Waters. Through the mediation of enhanced local primary productivity (Zhai et al., 2012), these fronts provide a habitat central to the distribution
45   and migration of Icelandic capelin schools (Ólafsdóttir and Rose, 2012), which in turn support higher food-web predators, such as Atlantic cod, whales and seabirds (Piatt and Methven, 1992; Vilhjálmsson, 2002; Davoren et al., 2003). Given its sensitive position relative to the AF and PF, the NIS is strategically located to study past variations in these frontal systems (c.f. Giraudeau et al., 2004), which can provide context for future changes in North Atlantic oceanic heat transport and for the sustainability of Icelandic fisheries (Árnason and Sigfússon, 2012).

50   An extensive collection of literature exists for the NIS that provides important datasets on temperature, productivity and sea ice changes during the Holocene (last 11.7 ka BP) (see Supplemental Table S1). Although these proxy records are influenced by additional environmental variables (i.e. seasonality, depth habitat of biota and/or nutrients) that can result in discrepancies between paleoceanographic interpretations, they consistently partition the Holocene into three divisions (e.g. Kristjánsdóttir et al., 2017). The major transitions occur at ~6.4 and 3.5 ka BP, with the interval in between reflecting the
55   highest levels of nutrient availability and local primary productivity, presumably related to the local stabilization of the Arctic Front (Giraudeau et al., 2004; Cabedo-Sanz et al., 2016; Kristjánsdóttir et al., 2017). Here, we leverage new high-resolution lipid biomarker and foraminiferal assemblage records to explore how Holocene changes in positions of the AF and PF are expressed in paleoceanographic and paleoproductivity proxies on the NIS. Our analysis builds on previous work by targeting two, high sedimentation rate sediment cores that are strategically located on the western and eastern NIS to capture regional
60   hydrographic gradients. The coupling of biogeochemical and traditional proxies with statistical analyses allows for more secure and detailed interpretations of paleoproductivity, temperature, and the position of the AF and PF during the Holocene.

2 Modern oceanography

The interactions between several water masses on the NIS results in a highly variable and complex hydrographic setting. Along the Denmark Strait, the North Iceland Irminger Current (NIIC) branches from the Irminger Current (IC) and transports warm

65 (>4 °C) and saline (>35 ‰) Atlantic Water along northwest Iceland (Stefánsson, 1962). These Atlantic Waters then meet Polar Water and drift ice that is carried south along the coast of Greenland by the East Greenland Current (EGC), where the boundary between the EGC and IC constitutes the local PF (Fig. 1). NIIC Atlantic Water can cool and mix with Polar Water in the Iceland Sea to form the submerged and westward flowing North Iceland Jet (NIJ, Våge et al., 2011; Jónsson and Valdimarsson, 2012). The East Iceland Current (EIC) branches off the EGC and carries cool Arctic water (1 to 4 °C) formed in the Iceland

70 Sea eastward along the NIS (Stefánsson, 1962). Although the EIC is generally ice free, it can occasionally advect EGC Polar Water and drift ice (c.f. Ólafsson, 1999). The boundary between the EIC and Atlantic Water is the local expression of the AF (Fig. 1). On the NIS, the water column becomes density stratified as the NIIC Atlantic Water converges with the Arctic/Polar Waters of the EIC. At the site of MD99-2269, NIIC Atlantic Water commonly forms the bottom water, but farther east at JR51-GC35 Atlantic Water is likely to occur as an intermediate watermass between Arctic Intermediate Water and surface

75 waters of the EIC (http://www.hafro.is/Sjora).

Although sea ice is dominantly transported from east Greenland to the NIS by the EGC and EIC, local production can also occur in extreme years (Ólafsson, 1999). The proximity of mean April and August instrumental sea ice edges (1870-1920 CE) to the NIS (Fig. 1) means that subtle changes in sea ice advection along the EGC/EIC can have profound changes in local climate (Ólafsson, 1999) as it limits the exchange of heat, gases and moisture between the ocean and atmosphere, in

80 addition to insulating the colder polar atmosphere from the relatively warmer ocean during winter (Harning et al., 2019). Strong Polar Water advection to the NIS stratifies the water column and limits mixing of nutrients carried in Atlantic Water (i.e. phosphate, nitrate, and silica) for renewal in the photic zone, thus limiting primary productivity (Stefánsson and Ólafsson, 1991). In contrast, an Arctic Water surface stimulates a spring phytoplankton bloom, whereas the dominance of Atlantic Water extends the bloom into the summer resulting in higher total seasonal biomass (Thordardóttir, 1984; Zhai et al., 2012).

85 3 Materials and Methods

3.1 Marine sediment cores

Two marine sediment cores separated by ~200 km on the NIS were selected for this study in order to capture the modern oceanographic gradients and ocean current positions. Marine sediment core MD99-2269 (66.63°N, 20.85°W, 365 mbsl) is located on the western NIS and under the primary influence of the NIIC Atlantic Water, whereas marine sediment core JR51-

90 GC35 (67.33°N, 16.70°W, 420 mbsl) lies on the eastern NIS and is mainly influenced by the EIC Arctic Water (Fig. 1). A variety of paleoceanographic datasets currently exist for MD99-2269, which rely on a securely-dated Holocene age model derived from 27 ^{14}C dates and paleomagnetic secular variation (Supplemental Table S1). Several similar corresponding datasets are also available for JR51-GC35, which use age control derived from 10 ^{14}C dates (see Supplemental Table S1). For

this study's inter-site comparisons, we focus on the biomarker records that have been analysed in both cores (Fig. 2, Bendle
95   and Rosell-Melé, 2007; Cabedo-Sanz et al., 2016; Kristjánsdóttir et al., 2017). Given that sedimentation rates are nearly linear
at both locations over the last 8 ka, we do not correct proxy records for sediment flux.

Alkenones are long-chain ketones produced by coccolithophore algae (class: *Prymnesiophyceae*) in the photic zone
that vary the number of unsaturation in response to sea surface temperature (SST) (Brassell et al., 1986; Prahl and Wakeham,
1987). We re-calculated SSTs from the original JR51-GC35 record (Bendle and Rosell-Melé, 2007) using the global $U^{K'}_{37}$
100   calibration (Müller et al., 1998)

$$(Eq. 1) \; SST = (U^{K'}_{37} - 0.044)/0.033$$

that removes the influence of $C_{37:4}$ alkenones, which dominate in low temperature environments (Prahl and Wakeham, 1987)
and may be more susceptible to diagenesis (Müller et al., 1998). Considering that the bloom and primary period of
phytoplankton production occurs during early spring along the NIS (Zhai et al., 2012), we interpret both SST records to hold
105   a spring seasonal bias.

The IP_{25} biomarker is a mono-unsaturated C_{25} highly-branched isoprenoid (HBI) alkene biosynthesized by certain
Arctic sea ice diatoms (Brown et al., 2014; Belt, 2018), whereas HBI III and HBI IV are tri-unsaturated C_{25} HBI alkenes
biosynthesized by some open-water diatoms (e.g. *Rhizosolenia* spp.) in the Arctic (Rowland et al., 2001; Belt et al., 2017).
Consequently, the presence of IP_{25} indicates the occurrence of seasonal sea ice along the sea ice margin whereas the presence
110   of HBI III reflects highly productive Marginal Ice Zones (MIZ) characterized by open water phytoplankton blooms (Belt et
al., 2015, 2019). Further, the proportion of HBI III to HBI IV can provide evidence for the spring phytoplankton bloom (Belt
et al., 2019).

3.2 Archaeal isoprenoid glycerol dibiphytanyl glycerol tetraethers

115   We present new subsurface temperature (subT) proxy records for each marine sediment core based on the distribution of
isoprenoid glycerol dibiphytanyl glycerol tetraether (GDGT). GDGTs are cell membrane lipids biosynthesized by marine
ammonia oxidizing Thaumarchaeota (Könneke et al., 2005; Schouten et al., 2013), which on the NIS vary in terms of their
cyclization (number of cyclopentane moieties) according to winter and/or annual subT (0-200 m, Harning et al., 2019), and
potentially to a lesser extent, ammonia oxidation rates (e.g. Hurley et al., 2016). Total lipids extracts (TLEs) were obtained
120   from freeze-dried marine sediment subsamples (~2-3 g, n=53 for MD99-2269, n=18 for JR51-GC35) by ultrasonication using
dichloromethane:methanol (2:1, v/v). TLEs were then suspended in hexane:isopropanol (99:1, v/v), sonicated, vortexed, and
filtered using a 0.45 µm PTFE syringe filter. Prior to instrumental analysis, samples were spiked with 10 ng of the C_{46} GDGT
internal standard (Huguet et al., 2006). Isoprenoid GDGTs were identified and quantified via high performance liquid
chromatography – mass spectrometry (HPLC-MS) a Thermo Scientific Ultimate 3000 HPLC system interfaced to a Q Exactive
125   Focus Orbitrap-Quadrupole MS after Harning et al. (2019). We adopt the TEX_{86}^{L} index (Kim et al., 2010) to quantify the
distribution of GDGTs

$$(Eq.\,2)\ TEX_{86}^{L} = \log\left(\frac{[GDGT-2]}{[GDGT-1]+[GDGT-2]+[GDGT-3]}\right)$$

and then convert to winter/annual subT based on a local Icelandic surface sediment calibration (Harning et al., 2019)

$$(Eq.\,3)\ subT = 27.898(TEX_{86}^{L}) + 22.723$$

130

3.3 Highly branched isoprenoids

We expand the HBI datasets of Cabedo-Sanz et al. (2016) (IP$_{25}$ and HBI III) by reporting corresponding records of HBI IV, a geometric isomer of HBI III (Fig. S1). HBI IV is often co-produced by the same open-water diatoms that produce HBI III (e.g. *Rhizosolenia* spp., Rowland et al., 2001) and the combination of the two has recently been shown to be a useful predictor of

135 spring phytoplankton blooms in the Barents Sea (Belt et al., 2019). Analysis of purified lipid fractions containing HBIs was carried out using gas chromatography–mass spectrometry (GC–MS) in total ion current (TIC) and selected ion monitoring (SIM) modes after Belt et al. (2019). HBI IV was identified based on its characteristic GC retention index (RI$_{HP5MS}$ = 2091) and mass spectrum (Belt et al., 2000; Belt, 2018). HBI IV quantification was achieved by comparison of mass spectral responses of its molecular ion (*m/z* 346) in SIM mode with those of the internal standard (9-OHD, *m/z* 350) and normalized

140 according to an instrumental response factor. HBI III and HBI IV datasets are then expressed through the following equation

$$(Eq.\,4)\ T_{25} = \left(\frac{[III]}{[III]+[IV]}\right)/0.62$$

where $T_{25} \geq 1$ provides a qualitative proxy measure for the occurrence of spring phytoplankton blooms (Belt et al., 2019). Moreover, Rowland et al. (2001) demonstrated a systematic increase in the amount of HBI III relative to HBI IV (i.e. higher T_{25}) with increasing growth rate of *Rhizosolenia setigera* cultured at higher temperatures.

145

3.4 Planktic and benthic foraminifera

The modern distributions of planktic and benthic foraminifera from marine surface sediment around Iceland provide a key baseline for interpreting local environmental changes (Johannessen et al., 1994; Rytter et al., 2002; Jennings et al., 2004). Based on this framework, downcore records from MD99-2269 have focused on certain indicator species at low- (benthic and

150 planktic species, Justwan et al., 2008) and high-resolution (planktic species, Cabedo-Sanz et al., 2016). We expand these records by presenting high-resolution and complete assemblage counts from 273 planktic and 295 benthic foraminifera samples from MD99-2269. The original high-resolution planktic records for *T. quinqueloba* and *N. pachyderma* (s) from MD99-2269 (Cabedo-Sanz et al., 2016) have been updated and represent the finalized dataset.

All sub-samples were prepared by wet sieving at 63 μm, 106 μm and 150 μm. Our dataset combines samples that had

155 been air-dried at 35 °C after sieving and stored dry together with ones that were not dried (Cabedo-Sanz et al., 2016). The former sample set was wetted prior to wet splitting, and all samples were reanalysed for assemblages in a buffered solution. Planktic (>150 μm) and benthic (>106 μm) foraminiferal assemblages are expressed as percentages of the total planktic and total benthic population. In addition to individual foraminiferal species profiles, we also use our assemblage datasets to estimate

bottom water temperature (BWT, benthic foraminiferal dataset) and sea surface temperature (SST, planktic foraminiferal
160   dataset). Temperature estimates were quantified using North Atlantic transfer functions (BWT, Sejrup et al., 2004; SST,
Pflaumann et al., 2003) and Weighted Averaging Partial Least Squares Regression (WAPLS) and Maximum Likelihood (ML)
techniques. Although the transfer functions assume a relationship with spring/summer temperature likely due to the seasonal
flux of phytodetritus that heterotrophic foraminifera feed on, foraminifera productivity likely occurs at other times of the year,
which result in annually integrated temperature records.

165

3.5 Statistical analyses

Step 1: To visualize long-term trends in proxy time series, we performed locally weighted smoothing (LOESS) to help
minimize the influence from outliers and short-term variability while retaining persistent shifts. The smoothing criterion for
each time series was selected automatically after optimization using generalized cross validation. Values along the resulting
170   LOESS curves were extracted using a 60 yr timestep, representing a balance between both the arithmetic mean (~90 yr) and
median (~30 yr) of first derivatives for each time series.

Step 2: To detect persistent step shifts within individual time series, we performed Sequential T-test Analysis of
Regime Shifts (STARS) on the LOESS-smoothed data (Rodionov, 2004, 2006). The algorithm was tuned to detect regime
shifts on millennial timescales by setting the cut-off length to 60, and we report the timing of shifts identified at the 95%
175   confidence level ($p \leq 0.05$). The timing of regime shifts is best interpreted as approximate, as their exact timing and magnitude
are affected by the chosen confidence level and cut-off length (e.g. Rodionov, 2006). Comparison of regime shift timing
between sediment cores should be approached with caution due to the variable resolution and quality of chronological control.

Step 3: To evaluate the relative similarity between select MD99-2269 productivity and temperature proxy time series,
we performed complete-linkage Agglomerative Hierarchical Clustering (AHC) using Dynamic Time Warping (DTW) distance
180   as a curve shape-based dissimilarity. In order to preserve the influence of short-term variability while rectifying missing data,
we avoided using LOESS smoothing and linearly interpolated the proxy records across all available horizons (600+ data
points).

4 Results

185   **4.1 Trends and regime shifts identified in existing proxy records**

Alkenone-derived $U^{K'}_{37}$ spring SST records from MD99-2269 (Kristjánsdóttir et al., 2017) and JR51-GC35 (Bendle and
Rosell-Melé, 2007) reveal different overall patterns of temperature variability during the last 8 ka. The record from MD99-
2269 is relatively lower in absolute spring SSTs as well as in the magnitude of shorter-term variability. It features four regime
shifts rather than five as found in JR51-GC35 (Fig. 2a-b). Both $U^{K'}_{37}$ records indicate that highest spring SSTs were achieved
190   during the earliest portion of the records with the lowest spring SSTs occurring variably between ~4 and 2 ka BP (Fig. 2a-b).
IP$_{25}$-derived sea ice records from both marine sediment cores (Cabedo-Sanz et al., 2016) show a similar pattern of low sea ice
occurrence in the early Middle Holocene followed by generally increasing amounts of seasonal sea ice towards present (Fig.

2e-f). Three positive regime shifts are identified in IP$_{25}$ record from MD99-2269, whereas four positive regime shifts are identified in JR51-GC35 (Fig. 2e-f). Similar to the IP$_{25}$ records, HBI III records from both marine sediment cores (Cabedo-

195   Sanz et al., 2016) show a similar pattern over the last 8 ka, with a period of relatively high concentrations between 6.1 and 3.8 ka BP compared to the periods before and after (Fig. 2g-h). Three regime shifts are identified in MD99-2269 whereas four are identified in JR51-GC35 (Fig. 2g-h).

4.2 Archaeal GDGTs

200   GDGTs are present above the detection limit in all sediment samples (Fig. S2). GDGT-0/crenarchaeol ratios around and below 2 (Fig. S2) indicate that the GDGT pool is not altered by methanogenic contributors (Blaga et al., 2009), and that Thaumarchaeota are the dominant producers of these GDGTs. The low standard error of the local Icelandic temperature calibration (±0.4 °C, Harning et al., 2019) increases our confidence in the observed changes in TEX$_{86}^{L}$-derived subT at both locations. For core MD99-2269, subT range from 6.7 to 3.1 °C and are subdivided by five regime shifts. The first regime shift

205   indicates an increase in subT whereas the subsequent four indicate continual decreases in subT at this site (Fig. 2c-d). SubT at JR51-GC35 range from 4.6 to 2.2 °C, and in contrast to MD99-2269, only show four regime shifts, which all indicate progressive decreases in subT. Although the timing of highest subT varies between the two core locations (~6 and 5 ka at MD99-2269 and by 8 ka in JR51-GC35), the timing of lowest subT occurs during the last 1 ka in both records (Fig. 2c-d).

210   ### 4.3 T$_{25}$

HBI IV was present above the detection limit in all sediment samples (Fig. S3). The T$_{25}$ records for both cores show similar trends, with highest values achieved during the early Middle Holocene and progressively lower values towards present (Fig. 2i-j). For marine sediment core MD99-2269, the T$_{25}$ record exhibits four negative regime shifts, whereas for marine sediment core JR51-GC35, the T$_{25}$ record exhibits five negative regimes shifts (Fig. 2i-j). The overall decreasing LOESS trends as well

215   as the consistently negative regimes shifts in both records indicate a generally continuous decline in pelagic productivity over the last 8 ka (e.g. Belt at al., 2019). Further, given that HBI III is produced at a relatively higher proportion under conditions of more rapid growth in some diatoms (e.g. *R. setigera,* Rowland et al., 2001), these records also suggest a long-term decrease in diatom growth rates.

220   ### 4.4 Planktic and benthic foraminifera

Seven planktic foraminiferal species were identified in the >150 µm size fraction and used for SST estimation (Fig. S4). Our reconstruction of planktic foraminifera assemblage and SST estimates include low- and high-resolution data before and after 8 ka BP, respectively (Fig. S4-S6). We focus on two planktic indicator species for our paleoceanographic discussion; *T. quinqueloba* and *N. pachyderma* (s). *T. quinqueloba* is an AF species (Johannessen et al., 1994; Volkmann, 2000; Pados and

225   Spielhagen, 2014) that shows highest abundance during the early Middle Holocene and lowest abundance during the Late Holocene, with four negative regime shifts (Fig. 3c). *N. pachyderma* (s) is a Polar Water species (Johannessen et al., 1994;

Jennings et al., 2004) that shows lowest abundances during the early Middle Holocene, and three positive shifts during the Late Holocene when its maximum abundance is achieved (Fig. 3d). In terms of foraminifera-reconstructed SST (S.E.=1.3 °C), there is an overall trend of cooling throughout the last 8 ka from ~10 °C to ~3 °C, although SST from 8 to ~4 ka BP and from

230   ~3 ka BP to present are relatively more stable than between 4 and 3 ka BP (Fig. 4b). Four negative regime shifts are identified throughout the SST record, the most pronounced of which occurs at ~4 ka BP (Fig. 4b).

In the benthic dataset, we focus on the two most abundant species, *Cassidulina neoteretis* and *Cassidulina reniforme*, for paleoceanographic interpretations. Around Iceland, *C. neoteretis* is abundant on the western NIS where it is associated with NIIC Atlantic Water and dramatically decreases eastward where Atlantic Intermediate Water forms the bottom water (Rytter

235   et al., 2002; Jennings et al., 2004). *C. reniforme* is an Arctic species prevalent on the NIS but has its highest abundance in the low-salinity fjords of NW Iceland (Rytter et al., 2002; Jennings et al., 2004). In our records, *C. neoteretis* shows maximum abundances during the Middle Holocene and exhibits three regime shifts throughout the last 8 ka (Fig. 3f). *C. reniforme* peaks during the early Middle Holocene and has five regime shifts throughout the last 8 ka (Fig. 3g). We note that another dominant species is *Nonionella iridea,* which formed up to 20 % of the benthic fauna (Fig. S5) and included in our statistical analyses

240   to better understand its environmental preferences (see Supporting Information Text S1). Thirty-three of the 65 species in the Sejrup et al. (2004) transfer function are present in MD99-2269, although neither *N. iridea* nor the agglutinated species were included (Sejrup et al., 2004). The BWT estimates are less variable than the foraminifera-based SST estimates, with temperatures generally falling between ~2.5 and 5 °C and maximum temperatures occurring at ~4 ka BP (S.E.=1.0 °C). Two positive regime shifts are identified in the Middle Holocene followed by two negative regime shifts during the Late Holocene,

245   consistent with the general long-term pattern of warming from 8 to ~4 ka BP and cooling from ~4 ka BP to present (Fig. 4d).

4.5 Agglomerative Hierarchical Clustering analysis

The AHC dendrogram of DTW distances shows that the 11 selected proxy records from MD99-2269 successfully separate into four clusters (Fig. 5). The first grouping of T_{25}, foraminifera SST, and TEX_{86}^{L} subT clusters proxies that are influenced

250   by annual near surface to surface temperatures. The spring $U^{K'}_{37}$ SST belongs to its own cluster likely due to seasonality differences that result in a relatively smaller range of temperature changes as well as warming since ~2 ka BP (Fig. 4a-c). The third grouping of HBI III, *T. quinqueloba* and, *N. iridea,* and to a slightly lesser extent, HBI IV, suggests that this cluster reflects a separate but dominant environmental variable on the NIS, likely pelagic productivity (see Supporting Information Text S1 for discussion on *N. iridea*). The close relationship of the productivity cluster (blue) to the temperature clusters (purple

255   and green) highlight the fact that SST and productivity are innately connected on the NIS as warmer Atlantic Water with sufficient vertical mixing often carry higher nutrient loads that stimulate primary production (e.g. Thordardóttir, 1984; Zhai et al., 2012). Finally, the fourth grouping of IP_{25}, *N. pachyderma* (s) and foraminifera BWT likely clusters cold proxy indicators, such as the sea ice biomarker IP_{25} and planktic foraminifera species associated with Polar Water and bottom waters. The fact that foraminifera BWT clusters in the fourth grouping may relate to the relatively depressed temperatures in the early portion

260   of the record, despite a negative trend from ~4 ka BP to present (Fig. 4d) that would be consistent with trends observed in the

aforementioned near surface temperature and productivity proxies (Figs. 3 and 4). In any case, we note that the similarity between BWT and Polar Water indicators is weaker than that between IP$_{25}$ and *N. pachyderma* (s).

5 Discussion

265 ### 5.1 Frontal proxies on the NIS

Modern distributions of *T. quinqueloba* along AF systems suggests that the species feeds in the high nutrient and productive waters within the warmer margins (Volkmann, 2000; Pados and Spielhagen, 2014). In prior work from MD99-2269, Cabedo-Sanz et al. (2016) used Principal Component Analysis to show that HBI III and *T. quinqueloba* were related, along with biogenic CaCO$_3$, as proxies for surface productivity. Our AHC analysis, which uses the updated *T. quinqueloba* record,

270 reinforces the relationship previously observed between HBI III and *T. quinqueloba* time series on the NIS (Fig. 5). Further, given the known environmental preferences of *T. quinqueloba,* we suggest that the NIS diatom producers of HBI III thrive in similar hydrographic conditions. Although we lack information on diatom sources in our study, the distribution of some HBI III-producing diatoms (i.e. *Rhizosolenia hebetata* f. *semispina*) do trace the AF's modern position (Oksman et al., 2019), and are important members of Arctic Water assemblages in the North Atlantic (Koç Karpuz & Schrader, 1990; Oksman et al.,

275 2019). Collectively, this evidence indicates that HBI III and *T. quinqueloba* track the migration of the AF along the NIS.

5.2 Environmental controls on benthic foraminifera Nonionella iridea

N. iridea is an often overlooked or missed constituent in benthic faunal assemblages (e.g. Sejrup et al., 2004) due its small size (Jennings et al., 2004) and because its abundance is underestimated using dry analyses. Experimental work indicates that N.

280 iridea may feed on seafloor phytodetritus and/or the associated suboxic-hypoxic bacterial populations that can develop, but only dominates the assemblage in response to pulsed phytodetritus delivery (Gooday and Hughes, 2002; Duffield et al., 2015). The wet picking techniques employed in our study allowed us to quantify downcore variations in N. iridea and better understand its environmental preferences and role in Icelandic benthic communities. N. iridea shows highest taxa abundance during the Middle Holocene, which features one negative regime shift. Lowest abundance occurred during the Late Holocene,

285 which features one negative regime shift followed by one positive (Fig. 6). Overall, the structure of the N. iridea, HBI III and T. quinqueloba records are similar (i.e. decreasing toward present) and the timing of regime shifts between them is consistent (Fig. 6). This notion of similarity is further supported by group clustering in our AHC analysis (Fig. 5). Although future studies including modern foraminifera distributions that include this species are still needed, this statistical evidence suggests that N. iridea's food supply may have been influenced by the presence of frontal systems and/or warmer waters. In other words, the

290 enhanced pelagic productivity of the AF likely resulted in increased export of phytodetritus to the seafloor where it could be consumed by N. iridea.

5.3 Migration of the Arctic Front and Polar Front
5.3.1 8 to 6.3 ka BP (northern distal Arctic Front)

295   In this interval, planktic foraminifera assemblages and the derived annual SST estimates indicate that NIIC Atlantic Water was

entering the MD99-2269 site, whereas Arctic Intermediate Water occupied the lower depths as indicated by the benthic fauna

and low BWT estimates (Fig. 4b-c and 7a). Coccolithophore assemblage data indicative of NIIC Atlantic Water from 8-7 ka

BP from the same core (Giraudeau et al., 2004) support the warm planktic foraminifera SST reconstruction. Both of our HBI

III records (Figs. 2g-h and 3a), as well as % *T. quinqueloba* (Fig. 3c), document low surface diatom productivity until ~6.1 ka

300   BP, which we interpret to reflect a northward position of the AF relative to the NIS (Fig. 7a). Although overall diatom biomass

was low, high T_{25} values indicate increased diatom growth rates (Fig. 3b), likely driven in part by higher temperatures (Fig. 5).

In addition, total benthic and planktic foraminifera counts were highest in this interval (Fig. S6), which may also indicate a

long ice-free season for production of some Arctic species. Although this interval of low phytoplankton productivity was

previously interpreted to reflect strong convection in the Iceland Sea and the production of Arctic Intermediate Water

305   (Giraudeau et al., 2004), we note that these interpretations are inconsistent with our planktic foraminifera assemblage dataset.

However, given the relatively high orbitally-induced seasonality at this time (Berger and Loutre, 1991), the periodic production

of cool and fresh North Icelandic Winter Water (Stefánsson, 1962) may have increased along the northern coastline. The

potential contribution of these local waters along with the distal position of the AF would have dampened surface productivity

for many frontal marine photosynthesizers (Fig. 7a).

310   Our datasets from MD99-2269 provide a comprehensive view of corresponding ocean temperatures on the western

NIS during this early Middle Holocene interval. $U^{K'}_{37}$ and foraminifera SST estimates show respectively high yet decreasing

spring and annual surface temperatures (Fig. 4a-b). In contrast, our TEX_{86}^{L}-derived subT and foraminifera BWT records show

depressed yet increasing temperatures (Fig. 4c-d). Hence, MD99-2269's temperature profile depicts a strong annual vertical

temperature gradient during the Early-Middle Holocene (~8 °C, Fig. 4e), resulting from stratification of Arctic Intermediate

315   Water at lower depths and NIIC Atlantic Water at the surface. At the JR51-GC35 core site, we also observe similarly high and

stable SST and relatively lower corresponding subT (Fig. 2b and 2d). However, a lack of BWT estimates in this core prevents

us from analysing the vertical temperature gradient on the eastern NIS. Comparison of TEX_{86}^{L} subT temperature records

between the western and eastern NIS show comparable absolute estimates (Fig. 4f), which likely reflects the invasion of NIIC

Atlantic Water across the surface to subsurface of the entire NIS (Fig. 7a).

320

5.3.2 6.3 to 3.4 ka BP (local stabilization of the Arctic Front)

At the beginning of this interval, planktic and benthic foraminifera indicate that NIIC Atlantic Water dominated the surface

whereas Arctic Intermediate Water occupied the lower depths on the western NIS (Fig. 3). At ~6.1 ka BP, abrupt increases in

HBI III and *T. quinqueloba* abundance from MD99-2269 indicate significantly enhanced pelagic primary production on the

325   western NIS, which although variable, is sustained to ~3.8 ka BP (Fig. 3). Although the HBI III record from JR51-GC35 shows

similar trends, the overall increase in inferred pelagic productivity is smaller (Fig. 2h). We interpret this spatial variability to

reflect that by 6.1 ka BP, the AF was positioned near MD99-2269 but never or rarely expanded eastward to JR51-GC35, and

that NIIC Atlantic Water was less of a contributor to the JR51-GC35 site (Fig. 7b). The increase in certain dinoflagellate and

coccolithophore algae species (e.g. *Coccolithus pelagicus*) have also been used to track the presence of the AF to MD99-2269
330   from 6.2 to 3.5 ka BP (Giraudeau et al., 2004; Solignac et., 2006). Not only do the dinocyst and *C. pelagicus* records further
support the timing of AF presence around MD99-2269, they also reflect short-term oscillations between NIIC Atlantic Water
and EIC Arctic Waters (Giraudeau et al., 2004; Solignac et al., 2006). Hence, although the AF was located around MD99-
2269 in this interval, its precise location on the NIS was not static.

In terms of temperature, $U^{K'}_{37}$ and planktic foraminifera proxies reflect a decrease in spring and annual SST,
335   respectively, beginning by ~5.3 ka BP followed by a second regime shift at ~4 ka BP (Fig. 4a-b). As nutrient availability was
presumably higher, diatom growth rate and cell division inferred from decreasing T_{25} was likely hampered by these decreasing
SSTs (Fig. 3b). In contrast to the SST records, TEX_{86}^L subT on the western NIS shows anomalous warmth from ~6 to 5 ka BP
(Fig. 4c). Interestingly, this peak subT warmth closely aligns with the initial increase of HBI III and *T. quinqueloba* and south-
eastward migration of the AF over the western NIS at MD99-2269 (Fig. 2). As shown by the foraminifera fauna and
340   temperature proxies, this frontal migration began to de-stratify the water column (Fig. 4e), which may have allowed warmer
water to advect to lower depths where Thaumarchaeota live (Fig. 7b). Alternatively, if Thaumarchaeota became stressed over
increased competition for NH_4^+ with frontal primary producers, their ammonia oxidation rates could decrease, which in culture
studies has been shown to increase GDGT-based temperatures (Hurley et al., 2016). If this is the case, the lack of increased
TEX_{86}^L subT changes at JR51-GC35 may suggest a reduced competition for nutrients and reinforce reduced advection of NIIC
345   Atlantic Water and a distal position of AF on the east NIS.

Following the regime shift at ~3.8 ka BP in the HBI III record from MD99-2269, the PF expanded southeast over the
NIS (Fig. 7c). At the surface, this is reflected by decreases in spring and annual SST, subT, BWT (Fig. 4a-d), decreases in %
T. quinqueloba at the expense of % *N. pachyderma* (s), lower diatom growth rates (decreasing T_{25}), increased IP_{25}-inferred sea
ice (Fig. 3), as well as continued thermal destratification (Fig. 4e). However, beneath the surface, benthic fauna show the
350   progressive submergence of the NIIC Atlantic Water under EIC Arctic Water (Fig. 3 and 7b). On the eastern NIS at JR51-
GC35, subT and IP_{25}-derived sea ice records also continue to decrease and increase, respectively, although to a lesser extent
than at MD99-2269 (Fig. 2). Combined with records of water mass distribution inferred from radiocarbon reservoir ages
(Eiríksson et al., 2004) and low-resolution planktic foraminifera assemblage and their $\delta^{18}O$ (Eiríksson et al., 2000; Knudsen et
al., 2004), these proxies reflect progressive cooling of EIC Arctic Water, rather than the shift in surface water source observed
355   at MD99-2269 (i.e. NIIC to EIC) (Fig. 4f). Additional records of ocean temperature and iceberg rafting along the NIS indicate
contemporaneous millennial-scale cooling during this interval (e.g. Moros et al., 2006; Jiang et al., 2015) likely linked to
changes in oceanic circulation, such as AMOC slowdown (Thornalley et al., 2009) and/or changes in atmospheric circulation
patterns (Orme et al., 2018).

One record that remains challenging to interpret during the Middle Holocene is the $U^{K'}_{37}$ SST at JR51-GC35. Bendle
360   and Rosell-Melé (2007) connected the high amplitude variability of $U^{K'}_{37}$ SST (Fig. 2b) to the strength of North Atlantic Deep
Water (NADW) formation and the Atlantic Meridional Overturning Circulation (AMOC). Although the amplitude of JR51-
GC35's $U^{K'}_{37}$ SST variability is inconsistent with our additional SST records, the timing of these SST changes is similar to

those inferred from paired Mg/Ca-δ^{18}O measurements of planktic foraminifera south of Iceland that reflect the relative strength of the AMOC and Subpolar Gyre (Thornalley et al., 2009). However, if changes in the AMOC explain SST variability along the eastern NIS, it would be expected that similar variations would also be present in the MD99-2269 record. One possibility that may explain the contrasting observations is that the warm NIIC positioned over MD99-2269 was fluctuating to and from the JR51-GC35 core site in accordance with variability in AMOC strength (Fig. 7b). Given that local coccolithophore communities have changed during the Holocene and that the species during this interval favor these dynamic surface conditions (Giraudeau et al., 2004), it is also possible that the high-amplitude changes in JR51-GC35's $U^{K'}_{37}$ SST may relate to algal community changes associated with the varying EIC vs NIIC source water.

5.3.3 3.4 ka BP to present (southward migration of Arctic Front)

Consistently low HBI III concentrations at both core sites throughout the remainder of the records suggest that the PF remained a local feature along the NIS during the Late Holocene (Fig. 2 and 7c). Further, planktic foraminifera (low % *T. quinqueloba* and high % *N. pachyderma* (s)) and rising concentrations of IP_{25} in MD99-2269 (Fig. 3) suggest that the EIC was now advecting more Polar Water relative to Arctic Water. Accordingly, there are regime shifts toward lower spring and annual SST and subT from ~2 to 1.3 ka BP (Fig. 4), and from toward *N. pachyderma* (s) dominance at ~1.6 ka BP (Fig. 3). Although the annual vertical temperature gradient on the western NIS had decreased to <1 °C from its early Middle Holocene maximum (Fig. 4e), Late Holocene cooling is observed at all depths (Fig. 4). The low SSTs in combinations with low pelagic nutrient availability is likely responsible for the lowest Holocene diatom biomass and growth rates observed in the HBI III and T_{25} records, respectively (Fig. 2). These observations fit well within the context of previous proxy research that has shown this period to be the coldest of the Holocene on the NIS (Eiríksson et al., 2000; Andersen et al., 2004; Jiang et al., 2015). Moreover, the periodic advection of sea ice around east Iceland and the increase in % *T. quinqueloba* in southwest Iceland marine sediment cores show that the AF had migrated to the southern coastline during the peak of this cooling from ~1760 to 1920 CE (i.e. Little Ice Age, Jennings et al., 2001).

Several regional proxy records, such as $U^{K'}_{37}$ in MD99-2269, have recently noted an upturn in the derived spring/summer SSTs over the last two millennia (e.g. Moossen et al., 2015; Kristjánsdóttir et al., 2017), possibly related to regional changes of atmospheric circulation (Orme et al., 2018). In light of the continued decrease in northern hemisphere summer insolation (Berger and Loutre, 1991) and growth of Icelandic ice caps that require local summer cooling (Larsen et al., 2011; Harning et al., 2016, 2018, 2020; Anderson et al., 2018; Geirsdóttir et al., 2019), Cabedo-Sanz et al. (2016) suggested that this "warming" may have been driven by either the presence of a thin freshwater lid that restricted mixing with deeper colder water and the supply of nutrients and/or a seasonal shift of alkenone production to later summer months following more persistent spring sea ice. Our foraminifera-derived annual SST from MD99-2269 (Fig. 4b) and foraminifera assemblage data (Fig. S4 and S5) suggest that despite possible changes in seasonality, cold and low salinity Polar Water formed the surface waters even during the spring/summer. These results support both of the mechanisms proposed by Cabedo-Sanz et al.

(2016) and suggest that drawing conclusions about regional spring SST warming over the last 2 ka should be approached with caution until the nuances of the individual proxies are better understood.

5.4 Controls on the Holocene migration of the Arctic and Polar Fronts

400 The dominant climate forcing during the Holocene has been the first-order, orbitally-driven decrease in northern hemisphere summer and annual insolation (Berger and Loutre, 1991). Our NIS SST records depict a similar first-order decrease (Fig. 4a-b), consistent with an insolation-driven reduction in northward heat transport (e.g. Andersen et al., 2004). Although variability in the strength of northward heat transport has been modulated by centennial to millennal-scale changes in NADW formation and the stability and strength of the AMOC (e.g. Thornalley et al., 2009), as well as possible changes in atmospheric circulation

405 (e.g. Orme et al., 2018), the progressive migration of the Arctic and Polar Fronts around Iceland suggest that insolation has also remained its primary control. Given that the movement of the North Atlantic frontal systems is manifested by regional temperature and productivity variability in the past, our new records may provide useful analogues for ongoing fossil fuel-driven warming.

Following the end of the Little Ice Age in ~1920 CE and a century of first-order warming (http://vedur.is), the AF

410 and PF have returned to positions along Greenland and proximal to the NIS (Fig. 7d), similar to those during the warm early Middle Holocene (Fig. 7b). Accordingly, enhanced primary productivity (increased *T. quinqueloba*) is noted in recent NIS sediment records, that in addition to the position of the AF and PF straddling the NIS, may also be driven by increased advection of Atlantic Water (Jónsson and Valdimarsson, 2012) and/or freshwater discharge from Greenland (Perner et al., 2019). As global temperature continue to rise and melting of the Greenland Ice Sheet accelerates, freshening of North Atlantic surface

415 waters is expected to continue. Although recent melt may help stimulate this productivity (Perner et al., 2019), there likely exists a threshold where too much freshening will restrict nutrient availability required for photosynthesis, as we observe during the Early Holocene (Fig. 7a). Further, the observed slowdown (Rahmstorf et al., 2015) and conceivable future shutdown of AMOC from Greenland melt (Bakker et al., 2016) may also result in a southward shift of North Atlantic frontal systems. Although more emprical and modeling research is needed to forecast future climate trajectories, our records highlight the

420 sensitivity of the AF and PF to temperature changes, which hold important implications for the local pelagic productivity and economies that it supports today.

6 Conclusions

- We present new TEX$_{86}^L$-derived subT and HBI productivity records from the western and eastern NIS, as well as new
425 high-resolution planktic and benthic foraminifera assemblage (and corresponding temperature) records from the western NIS; all covering the last 8 ka.
- The Arctic Front, a zone of intensified pelagic productivity (as indicated by HBI III and % *T. quinqueloba*), moderate phytoplankton growth rates and warmer waters, stabilized on the NIS by ~6.1 ka BP, with greater influence on the west than the east. By ~3.8 ka BP, the Arctic Front migrated south of the NIS, allowing for cold, Arctic/Polar Water

430   associated with the Polar Front (as indicated by IP$_{25}$ and *N. pachyderma* (s)) to dominate the NIS for the Late Holocene.

- Vertical temperature gradients on the western NIS were largest during the early Middle Holocene and progressively decreased to the lowest temperature gradients during the Late Holocene. Longitudinal temperature gradients suggest that warmer NIIC Atlantic Water was more influential on the west compared to the eastern NIS where cooler EIC Arctic Water dominated.

- The Holocene migration of the AF and PF has been primarily controlled by first-order decreases in northern hemisphere insolation, but the productivity it supports is also sensitive to freshening of surface waters. The future balance between these two variables will shape how the local configuration of marine fronts in the North Atlantic will develop under continued regional warming.

Data availability

Upon publication data will be uploaded to the PANGAEA database. During the review of the manuscript, data will be made available upon reasonable request to the authors.

Declaration of Competing Interests

The authors declare that they have no conflict of interest.

Acknowledgements

We extend great thanks to the scientific parties and crews of the RRS *James Clark Ross* and R/V *Marion Dufresne II* cruises for initial sediment core collection, as well as the numerous authors of previous studies (and in particular Dr. John T. Andrews) who have contributed to both cores' comprehensive datasets and planted the seeds for continued research. We also thank Dr. Suzanne Maclachlan at the British Ocean Sediment Core Research Facility (BOSCORF), UK, for making sediments available from core JR51-GC35 and Dr. Patricia Cabedo-Sanz for providing us with HBI IV biomarker data. University of Colorado students Allyson Rugg, Ian Courtney, Kelly Curtis, Jessica Scherer and Kylie Smith counted the foraminiferal assemblages in MD99-2269, expanding on the initial assemblage data produced by Nancy Weiner. This study has been supported by the Icelandic Research Council (RANNIS) Grant of Excellence #141573-051 to ÁG and co-authors, as well as internal University of Colorado Boulder funds to JS.

Author Contributions

DJH conceived the study following discussions with AJ and STB. AJ led foraminifera analyses, DK extracted TLEs and performed statistical analyses, and DJH performed GDGT analyses. STB, ÁG and JS supported analytical expenses. DJH wrote the manuscript with contributions and discussion of data interpretations from all co-authors.

References

Andersen, C., Koç, N., Jennings, A.E., and Andrews, J.T.: Nonuniform response of the major surface currents in the Nordic
465 Seas to insolation forcing: Implications for the Holocene climate variability. Paleoceanography, 19, 1-16, 2004.

Anderson, L.S., Flowers, G.E., Jarosch, A.H., Aðalgeirsdóttir, G.Th., Geirsdóttir, Á., Miller, G.H., Harning, D.J.,
Thorsteinsson, T., Magnússon, E., and Pálsson, F.: Holocene glacier and climate variations in Vestfirðir, Iceland, from the
modeling of Drangajökull ice cap. Quat. Sci. Rev., 190, 39-56, 2018.
470
Árnason, R., and Sigfússon, Þ.: Þýðing sjávarklasans í íslensku efnahagslífi. Published by Islandsbanki, Reykjavík, 2012.

Bakker, P., Schmittner, A., Lenaerts, J.T.M., Abe-Ouchi, A., Bi, D., van den Broeke, M.R., Chan, W.-L, Hu, A., Beadling,
R.L., Marsland, S.J., Mernild, S.H., Saenko, O.A., Swingedouw, D., Sullivan, A., and Yin, J.: Fate of the Atlantic meridional
475 overturning circulation: strong decline under continued warming and Greenland melting. Geophys. Res. Lett., 43, 12252-
12260, 2016.

Belkin, I.M.: Propagation of the ''Great Salinity Anomaly" of the 1990s around the northern North Atlantic. Geophys. Res.
Lett., 31, L08306, 2004.
480
Belkin, I.M., Cornillon, P.C., and Sherman, K.: Fronts in Large Marine Ecosystems. Prog. Oceangr., 81, 223-236, 2009.

Belt, S.T.: Source-specific biomarkers as proxies for Arctic and Antarctic sea ice: Org. Geochem., 125, 277–298, 2018.

485 Belt, S.T., Allard, W.G., Massé, G., Robert, J.-M., and Rowland, S.J., 2000. Highly branched isoprenoids (HBIs): Identification
of the most common and abundant sedimentary isomers. Geochim. Cosmochim. Acta., 64, 3839-3851.

Belt, S.T., Brown, T.A., Navarro Rodriguez, A., Cabedo Sanz, P., Tonkin, A., and Ingle, R.: A reproducible method for the
extraction, identification and quantification of the Arctic sea ice proxy IP25 from marine sediments. Anal. Methods, 4, 705–
490 713, 2012.

Belt, S.T., Brown, T.A., Smik, L., Tatarek, A., Wiktor, J., Stowasser, G., Assmy, P., Allen, C.S., and Husum, K.: Identification
of C_{25} highly branched isoprenoid (HBI) alkenes in diatoms of the genus *Rhizosolenia* in polar and sub-polar marine
phytoplankton. Org. Geochem., 110, 65–72, 2017.
495
Belt, S.T., Cabedo-Sanz, P., Smik, L., Rodriguez-Navarro, A., Berben, S.M.P., Knies, J., and Husum, K.: Identification of
paleo Arctic winter sea ice limits and the marginal ice zone: Optimised biomarker-based reconstructions of late Quaternary
Arctic sea ice. Earth Planet. Sci. Lett., 431, 127-139, 2015.

Belt, S.T., Smik, L., Köseoğlu, D., Knies, J., and Husum, K.: A novel biomarker-based proxy for the spring phytoplankton
500 bloom in Arctic and sub-arctic settings – HBI T_{25}. Earth Planet. Sci. Lett., 523, 115703, 2019.

Bendle, J.A.P., and Rosell-Melé, A.: High-resolution alkenone sea surface temperature variability on the North Icelandic Shelf:
implications for Nordic Seas palaeoclimatic development during the Holocene. Holocene, 17, 9-24, 2007.

Berger, A., and Loutre, M.F.: Insolation values for the climate of the last 10 million years.
505 Quat. Sci. Rev., 10, 297-317, 1991.

Blaga, C.I., Reichart, G.-J., Heiri, O., and Sinninghe Damsté, J.S.: Tetraether membrane lipid distribution in water- column particulate matter and sediments: A study from 47 European lakes along a north-south transect. J. Paleolimnol., 41, 535–540, 2009.

510   Brassell, S.C., Eglington, G., Marlowe, I.T., Pflaumann, U., and Sarnthein, M.: Molecular stratigraphy: a new tool for climatic assessment. Nature, 320, 129-133, 1986.

Brown, T.A., Belt, S.T., Tatarek, A., and Mundy, C.J.: Source identification of the Arctic sea ice proxy IP$_{25}$. Nat. Comm. 5, 1-7, 2014.

515

Buckley, M.W., and Marshall, J.: Observations, inferences, and mechanisms of the Atlantic Meridional Overturning Circulation: A review. Rev. Geophys., 54, 5-63, 2015.

Cabedo-Sanz, P., Belt, S.T., Jennings, A.E., Andrews, J.T., and Geirsdóttir, Á.: Variability in drift ice export from the Arctic
520   Ocean to the North Icelandic Shelf over the last 8000 years: A multi-proxy evaluation. Quat. Sci. Rev., 146, 99-115, 2016.

Davoren, G.K., Montevecchi, W.A., and Anderson, J.T.: Distributional patterns of a marine bird and its prey: habitat selection based on prey and conspecific behaviour. Mar. Ecol. Prog. Ser., 256, 229–242, 2003.

525   Duffield, C.J., Hess, S., Norling, K., and Alve, E.: The response of *Nonionella iridea* and other benthic foraminifera to "fresh" organic matter enrichment and physical disturbance. Mar. Micropaleontol., 120, 20-30, 2015.

Eiríksson, J., Knudsen, K.L., Haflidason, H., and Henriksen, P.: Late-glacial and Holocene palaeoceanography of the North Icelandic Shelf. J. Quat. Sci., 15, 23-42, 2000.

530

Eiríksson, J., Larsen, G., Knudsen, K.L., Heinemeier, J., and Símonarson, L.A.: Marine reservoir age variability and water mass distribution in the Iceland Sea. Quat. Sci. Rev., 23, 2247-2268, 2004.

Geirsdóttir, Á., Miller, G.H., Andrews, J.T., Harning, D.J., Anderson, L.S., Larsen, D.J., Florian, C., and Thordarson, T.: The
535   onset of Neoglaciation in Iceland and the 4.2 ka event. Climate Past Diss., 15, 25-40, 2019.

Giraudeau, J., Jennings, A.E., and Andrews, J.T.: Timing and mechanisms of surface and intermediate water circulation changes in the Nordic Sea over the last 10000 cal years: A view from the North Iceland Shelf. Quat. Sci. Rev., 23, 2127-2139, 2004.

540

Gooday, A.J., and Hughes, J.A.: Foraminifera associated with phytodetritus deposits at the bathyal site in the northern Rockall Trough (NE Atlantic): seasonal contrasts and a comparison of stained and dead assemblages. Mar. Micropaleontol., 46, 83-110, 2002.

545   Harning, D.J., Geirsdóttir, Á., and Miller, G.H.: Punctuated Holocene climate of Vestfirðir, Iceland, linked to internal/external variables and oceanographic conditions. Quat. Sci. Rev., 189, 31-42, 2018.

Harning, D.J., Geirsdóttir, Á., Miller, G.H., and Anderson, L.S.: Episodic expansion of Drangajökull, Vestfirðir, Iceland over the last 3 ka culminating in its maximum dimension during the Little Ice Age. Quat. Sci. Rev., 152, 118-131, 2016.

550

Harning, D.J., Andrews, J.T., Belt, S.T., Cabedo-Sanz, P., Geirsdóttir, Á., Dildar, N., Miller, G.H., and Sepúlveda, J.: Sea ice control on winter subsurface temperatures of the North Iceland Shelf during the Little Ice Age: A TEX$_{86}$ calibration case study. Paleoceanogr. Paleoclimatol., 34, 1006-2021, 2019.

555   Harning, D.J., Curtin, L., Geirsdóttir, Á., D'Andrea, W.J., Miller, G.H., and Sepúlveda, J.: Lipid biomarkers quantify Holocene summer temperature and ice cap sensitivity in Icelandic lakes. Geophys. Res. Lett., 47, 1-11, 2020.

Huguet, C., Hopmans, E.C., Febo-Ayala, W., Thompson, D.H., Sinninghe Damsté, J.S., and Schouten, S.: An improved method to determine the absolute abundance of glycerol dibiphytanyl glycerol tetraether lipids. Org. Geochem., 37, 1036-
560   1041, 2006.

Hurley, S.J., Elling, F.J., Könneke, M., Buchwald, C., Wankel, S.D., Santoro, A.E., Lipp, J.S., Hinrichs, K.-U., and Pearson, A.: Influence of ammonia oxidation rate on thaumarchaeal lipid composition and the TEX$_{86}$ temperature proxy. Proc. Natl Acad. Sci., 113, 7762-7767, 2016.
565

Jennings, A.E., Hagen, S., Hardardóttir, J., Stein, R., Ogilvie, A.E.J., and Jonsdóttir, I.: Oceanographic change and terrestrial human impacts in a post A.D. 1400 sediment record from the southwest Iceland shelf. Clim. Chang., 48, 83-100, 2001.

Jennings, A.E., Weiner, N.J., Helgadóttir, G., and Andrews, J.T.: Modern foraminiferal faunas of the southwestern to northern
570   Iceland Shelf: oceanographic and environmental controls. J. Foram. Res., 34, 180-207, 2004.

Jiang, H., Muscheler, R., Björck, S., Seidenkrantz, M.-S., Olsen, J., Sha, L., Sjolte, J., Eiríksson, J., Ran., L., Knudsen, K.-L., and Knudsen, M.F.: Solar forcing of Holocene summer sea-surface temperatures in the northern North Atlantic. Geology, 43, 2-5, 2015.
575

Johannessen, T., Jansen, E., Flatøy, A., and Ravelo, A.C.: The Relationship between Surface Water Masses, Oceanographic Fronts and Paleoclimatic Proxies in Surface Sediments of the Greenland, Iceland, Norwegian Seas, Carbon Cycling in the Glacial Ocean: Constraints on the Ocean's Role in Global Change. Springer, pp. 61-85, 1994.

580   Jónsson, S., and Valdimarsson, H.: Water mass transport variability to the North Iceland Shelf, 1994-2010. ICES J. Mar. Sci., 69, 809-815, 2012.

Justwan, A., Koc, N., and Jennings, A.E.: Evolution of the Irminger and East Icelandic Current systems through the Holocene, revealed by diatom-based sea surface temperature reconstructions. Quat. Sci. Rev., 27, 1571-1582, 2008.
585

Kim, J.-H., van der Meer, J., Schouten, S., Helmke, P., Willmott, V., Sangiorgi, F., Koc, N., Hopmans, E.C., and Sinninghe Damsté, J.S.: New indices and calibrations derived from the distribution of crenarchaeal isoprenoid tetraether lipids: Implications for past sea surface temperature reconstructions. Geochim. Cosmochim. Acta, 74, 4639-4653, 2010.

590   Knudsen, K.L., Jiang, H., Jansen, E., Eiríksson, J., Heinemeier, J., and Seidenkrantz, M.S.: Environmental changes off North Iceland during the deglaciation and the Holocene: foraminifera, diatoms and stable isotopes. Mar. Micropaleontol., 50, 273-305, 2004.

Koç Karpuz, N., and Schrader, H.: Surface sediment diatom distribution and Holocene paleotemperature variations in the
595   Greenland, Iceland and Norwegian Sea. Paleoceanography, 5, 557-580,1990.

Könneke, M., Bernhard, A.E., de la Torre, J.R., Walker, C.B., Waterbury, J.B., and Stahl, D.A.: Isolation of an autotrophic ammonia-oxidizing marine archaeon. Nature, 437, 543-546, 2005.

600   Kristjánsdóttir, G.B., Moros, M., Andrews, J.T., and Jennings, A.E.: Holocene Mg/Ca, alkenones, and light stable isotope measurements on the outer North Iceland shelf (MD99-2269): A comparison with other multi-proxy data and sub-division of the Holocene. Holocene, 26, 55-62, 2017.

Larsen, D.J., Miller, G.H., Geirsdóttir, Á., and Thordarson, T., 2011. A 3000-year varved record of glacier activity and climate
605 change from the proglacial lake Hvítárvatn, Iceland. Quat. Sci. Rev., 30, 2715-2731, 2011.

Malmberg, S.-A., and Jonsson, S.: Timing of deep convection in the Greenland and Iceland Seas. ICES J. Mar. Sci., 54, 300–309, 1997.

610 Minobe, S., Kuwano-Yoshida, A., Komori, N., Xie, S.-P., and Small, R.J.: Influence of the Gulf Stream on the troposphere. Nature, 452, 206–209, 2008.

Moossen, H., Bendle, J., Seki, O., Quillmann, U., and Kawamura, K.: North Atlantic Holocene climate evolution recorded by high-resolution terrestrial and marine biomarker records. Quat. Sci. Rev., 129, 111-127, 2015.
615

Moros, M., Andrews, J.T., Eberl, D.D., and Jansen, E.: Holocene history of drift ice in the northern North Atlantic: Evidence for differential spatial and temporal modes. Paleoceanography, 21, 1-10, 2006.

Müller, P.J., Kirst, G., Ruhland, G., von Storch, I., and Rosell-Melé, A.: Calibration of the alkenone paleotemperature index
620 $U^{K'}_{37}$ based on core-tops from the eastern South Atlantic and the global ocean (60ºN-60ºS). Geochim. Cosmochim. Acta, 62, 1757-1772, 1998.

Oksman, M., Juggins, S., Miettinen, A., Witkowski, A., and Weckström, K.: The biogeography and ecology of common diatom species in the northern North Atlantic, and their implications for paleoceanographic reconstructions. Mar. Micropaleontol.,
625 148, 1-28, 2019.

Ólafsdóttir, A.H., and Rose, G.A.: Influences of temperature, bathymetry and fronts on spawning migration routes of Icelandic capelin (*Mallotus villosus*). Fish. Oceanogr., 21, 182-198, 2012.

630 Ólafsson, J.: Connections between oceanic conditions off N-Iceland, Lake Mývatn temperature, regional wind direction variability and the North Atlantic oscillation. Rit Fiskideildar, 16, 41-57, 1999.

Orme, L.C., Miettinen, A., Divine, D., Husum, K., Pearce, C., Van Nieuwenhove, N., Born, A., Mohan, R., and Seidenkrantz, M.-S.: Subpolar North Atlantic sea surface temperature since 6 ka BP: Indications of anomalous ocean-atmosphere interactions
635 at 4-2 ka BP. Quat. Sci. Rev., 194, 128-142, 2018.

Pados, T., and Spielhagen, R.F.: Species distribution and depth habitat of recent planktic foraminifera in Fram Strait, Arctic Ocean. Polar Res., 33, 1-12, 2014.

640 Perner, K., Moros, M., Otterå, O.H., Blanz, T., Schneider, R.R., and Jansen, E.: An oceanic perspective on Greenland's recent freshwater discharge since 1850. Sci. Rep., 9, 1-10, 2019.

Pflaumann, U., Sarnthein, M., Chapman, M., d'Abreu, L., Funnell, B., Huels, M., Kiefer, M., Maslin, M., Schulz, H., Swallow, J., van Kreveld, S., Vautravers, M., Vogelsang, E., and Weinelt, M.: Glacial North Atlantic: sea-surface conditions
645 reconstructed by GLAMAP 2000. Paleoceanogr. Paleoclimatol., 18, 1065, 2003.

Piatt, J.F., and Methven, D.A.: Threshold foraging behaviour of baleen whales. Mar. Ecol. Prog. Ser., 84, 205–210, 1992.

Prahl, F.G., and Wakeham, S.G.: Calibration of unsaturation in long-chain ketone compositions for palaeotemperature
650 assessment. Nature, 330, 533-537, 1987.

Rahmstorf, S., Box, J.E., Feulner, G., Mann, M.E., Robinson, A., Rutherford, S., and Schaffernicht, E.J.: Exceptional twentieth-century slowdown in Atlantic Ocean overturning circulation. Nat. Clim. Chang., 5, 475-480, 2015.

655   Rodionov, S.N.: A sequential algorithm for testing climate regime shifts. Geophys. Res. Lett., 31, L09204, 2004.

Rodionov, S.N.: Use of prewhitening in climate regime shift detection. Geophys. Res. Lett. 33, 1-4, 2006.

Rowland, S.J., Allard, W.G., Belt, S.T., Massé, G., Robert, J.M., Blackburn, S., Frampton, D., Revill, A.T., and Volkman,
660   J.K.: Factors influencing the distributions of polyunsaturated terpenoids in the diatom, Rhizosolenia setigera. Phytochemistry,
58, 717-728, 2001.

Rytter, F., Knudsen, K.L., Seidenkrantz, M.-S., and Eiríksson, J.: Modern distribution of benthic foraminifera on the North
Iceland shelf and slope. J. Foram. Res., 32, 217–244, 2002.
665
Schouten, S., Hopmans, E.C., and Sinninghe Damsté, J.S.: The organic geochemistry of glycerol dialkyl glycerol tetraether
lipids: A review. Org. Geochem., 54, 19-61, 2013.

Sejrup, H.P., Birks, H.J.B., Kristensen, D.K., and Madsen, H.: Benthonic foraminiferal distributions and quantitative transfer
670   functions for the northwest European continental margin. Mar. Micropaleontol., 53, 197-226, 2004.

Small, R.J., deSzoeke, S.P., Xie, S.P., O'Neill, L., Seo, H., Song, Q., Cornillon, P., Spall, M., and Minobe, S.: Air–sea
interaction over ocean fronts and eddies. Dynam. Atmos. Ocean., 45, 274–319, 2008.

675   Solignac, S., Giraudeau, J., and de Vernal, A.: Holocene sea surface conditions in the western North Atlantic: Spatial and
temporal heterogeneities. Paleoceanography, 21, 1-6, 2006.

Stefánsson, U.: North Icelandic Waters. Rit Fiskideildar III. Bind, vol 3, 1962.

680   Stefánsson, U., and Ólafsson, J.: Nutrients and fertility of Icelandic waters. Rit fiskideildar, 1-56, 1991.

Swift, J.H., and Aagaard, K.: Seasonal transitions and water mass formation in the Iceland and Green- land seas. Deep-Sea
Res., 28A, 1107-1129, 1981.

685   Thordardóttir, T.: Primary production north of Iceland in relation to water masses in May–June 1970–1989. ICES CM 1984/
L:20, 17p, 1984.

Thornalley, D.J.R., Elderfield, H., and McCave, I.N.: Holocene oscillations in temperature and salinity of the surface subpolar
North Atlantic. Nature, 457, 711-714, 2009.
690
Våge, K., Pickart, R.S., Spall, M.A., Valdimarsson, H., Jónsson, S., Torres, D. J., Østerhus, S., and Eldevik, T.: Significant
role of the North Icelandic Jet in the formation of Denmark Strait overflow water. Nat. Geosci., 4, 723–727, 2011.

Vilhjálmsson, H.: Capelin (*Mallotus villosus*) in the Ice-land–East Greenland–Jan Mayen ecosystem. ICES J. Mar. Sci., 59,
695   870–883, 2002.

Volkmann, R.: Planktic foraminifers in the outer Laptev Sea and the Fram Strait—modern distribution and ecology. J.
Foramin. Res., 30, 157–176, 2000.

700   Zhai, L., Gudmundsson, K., Miller, P., Peng, W., Guðfinnsson, H., Debes, H., Hátún, H., White III, G. N., Hernández Walls,
R., Sathyendranath, S., and Platt, T.: Phytoplankton phenology and production around Iceland and Faroes. Continental Shelf
Res., 37, 15– 25, 2012.
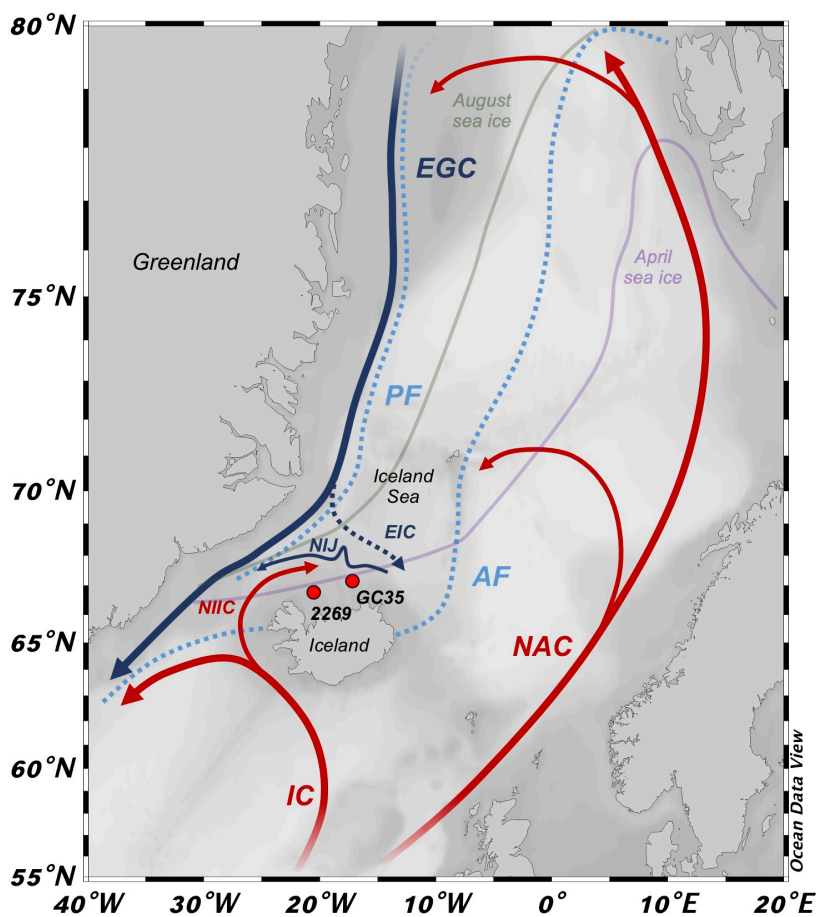
Figure 1: Overview map. Northern North Atlantic region with modern simplified position of ocean currents (bold lines), Arctic and Polar Fronts (dotted light blue lines, AF and PF, respectively), and mean 1870-1920 CE seasonal sea ice edges (April = purple, August = green, http://nsidc.org). Atlantic currents are red: IC = Irminger Current, NIIC = North Iceland Irminger Current, and NAC = North Atlantic Current. Polar currents are blue: EGC = East Greenland Current and NIJ = North Iceland Jet. Arctic currents are dashed blue: EIC = East Iceland Current. Marine sediment core locations marked by red circles with abbreviated core names (i.e. MD99-2269=2269 and JR51-GC35=GC35).
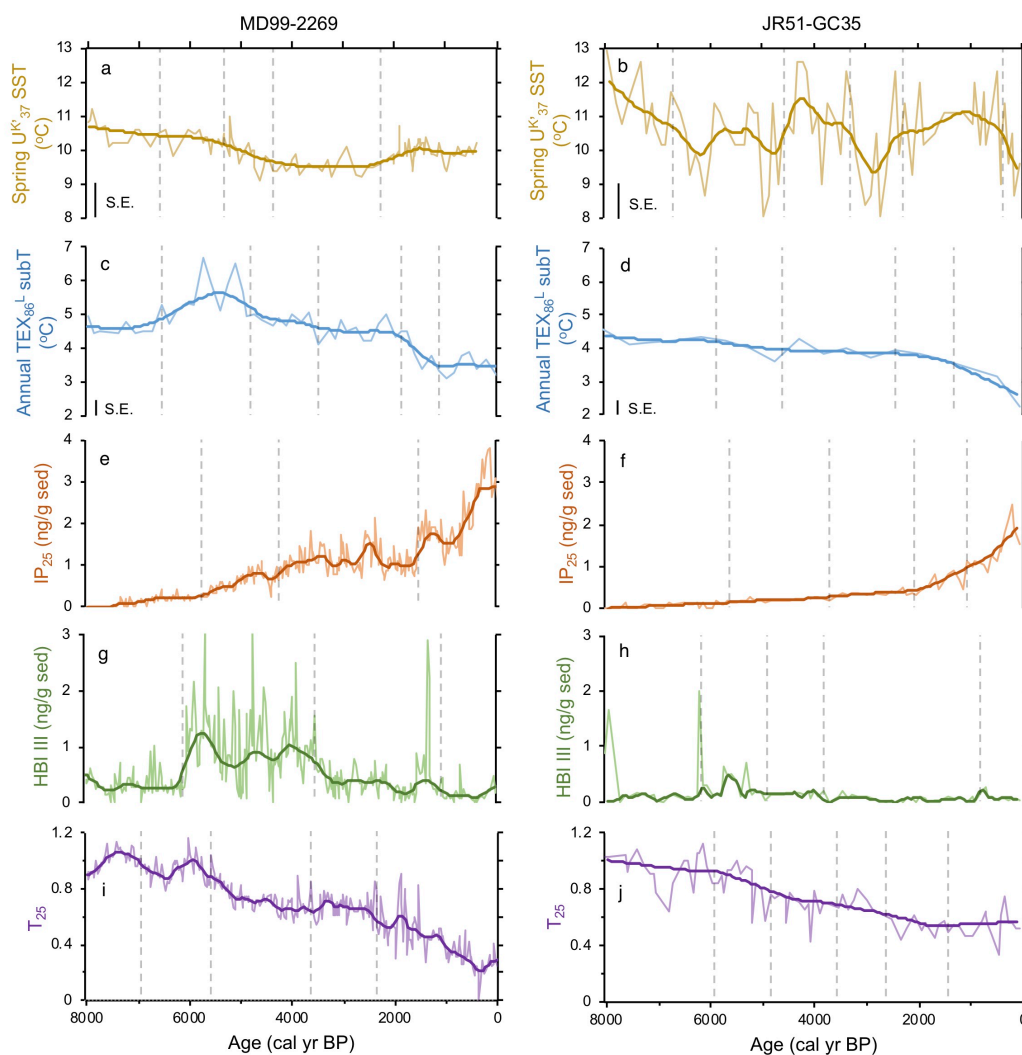
Figure 2: Shared lipid biomarker records for marine sediment cores MD99-2269 (left) and JR51-GC35 (right). a-b) alkenone-derived SST (Bendle and Rosell-Melé, 2007; Kristjánsdóttir et al., 2017), c-d) GDGT-derived sub T, e-f) IP_{25} proxy for seasonal sea ice (Cabedo-Sanz et al., 2016), g-h) HBI III proxy for highly productive MIZ (Cabedo-Sanz et al., 2016), and i-j) T_{25} proxy for spring phytoplankton bloom growth rates. Y-axes have the same scale per proxy for easier visualization of proxy records between the two sites. Vertical dashed gray lines indicate regime shifts statistically identified in the LOESS-smoothed records.
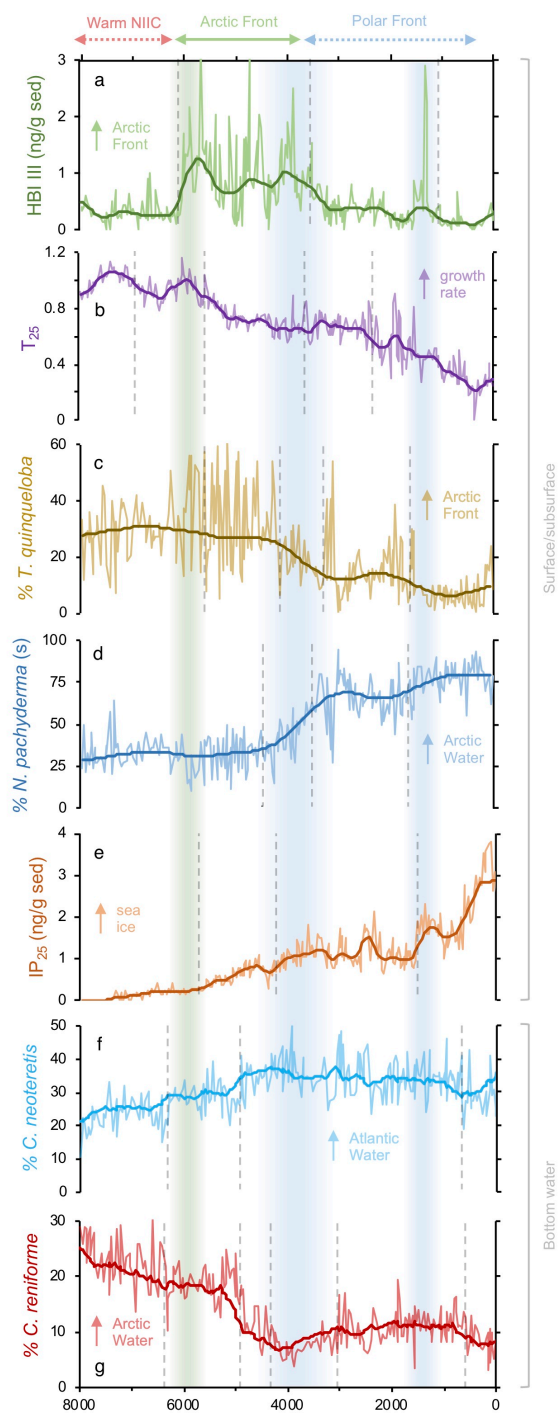
720 **Figure 3: Qualitative productivity proxies from marine sediment core MD99-2269.** a) HBI III proxy for highly productive MIZ and marine fronts (Cabedo-Sanz et al., 2016), b) T$_{25}$ proxy for spring phytoplankton bloom growth rates, c) % *T. quinqueloba* planktic foraminifera, d) % *N. pachyderma* (s) planktic foraminifera, e) IP$_{25}$ proxy for seasonal sea ice presence (Cabedo-Sanz et al., 2016), f) % *C. neoteretis* benthic foraminifera, and g) % *C. reniforme* benthic foraminifera. Vertical dashed gray lines indicate regime shifts statistically identified in the LOESS-smoothed records. Vertical green bar indicates the timing of Polar Front establishment in the early Middle Holocene.

725 The first blue bar (Middle Holocene) indicates the southward migration and departure of the Arctic Front from the NIS, and the second (Late Holocene) blue bar indicates a period of further cooling interpreted from the proxy regime shifts.
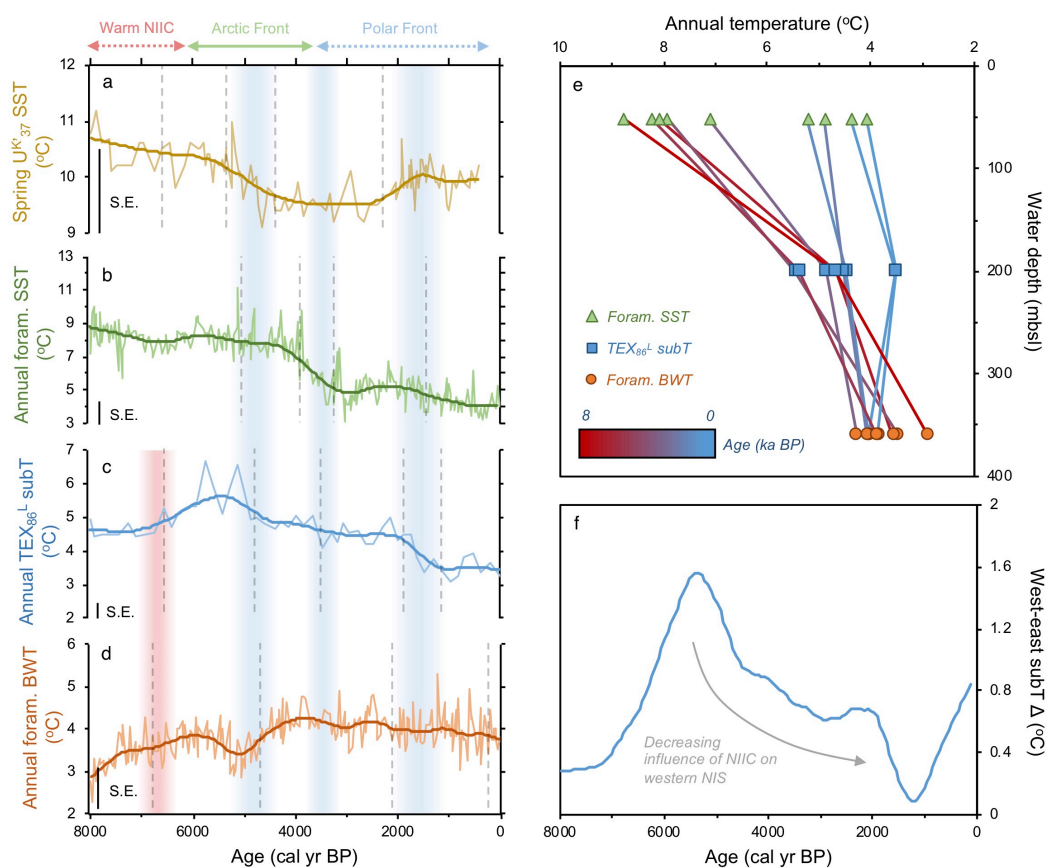
Figure 4: Quantitative temperature proxies from marine sediment core MD99-2269. a) U$^{K'}_{37}$ SST (Kristjánsdóttir et al., 2017), b)

730 foraminifera assemblage SST, c) TEX$_{86}^{L}$ subT, and d) foraminifera assemblage BWT. All panels show the corresponding calibration standard errors (S.E.) in the bottom left. Vertical dashed gray lines indicate regime shifts statistically identified in the LOESS-smoothed records. Vertical red bar indicates warming in subT (c) and BWT (d), whereas vertical blue bars indicate periods of progressive cooling expressed in proxy regime shifts. e) vertical temperature gradient inferred from MD99-2269 LOESS-smoothed annual temperature proxies in 1000-year time slices (blue graded lines) and f) longitudinal subT gradient inferred from the difference between LOESS-smooth TEX$_{86}^{L}$ records on the

735 west (MD99-2269) and east (JR51-GC35) NIS.
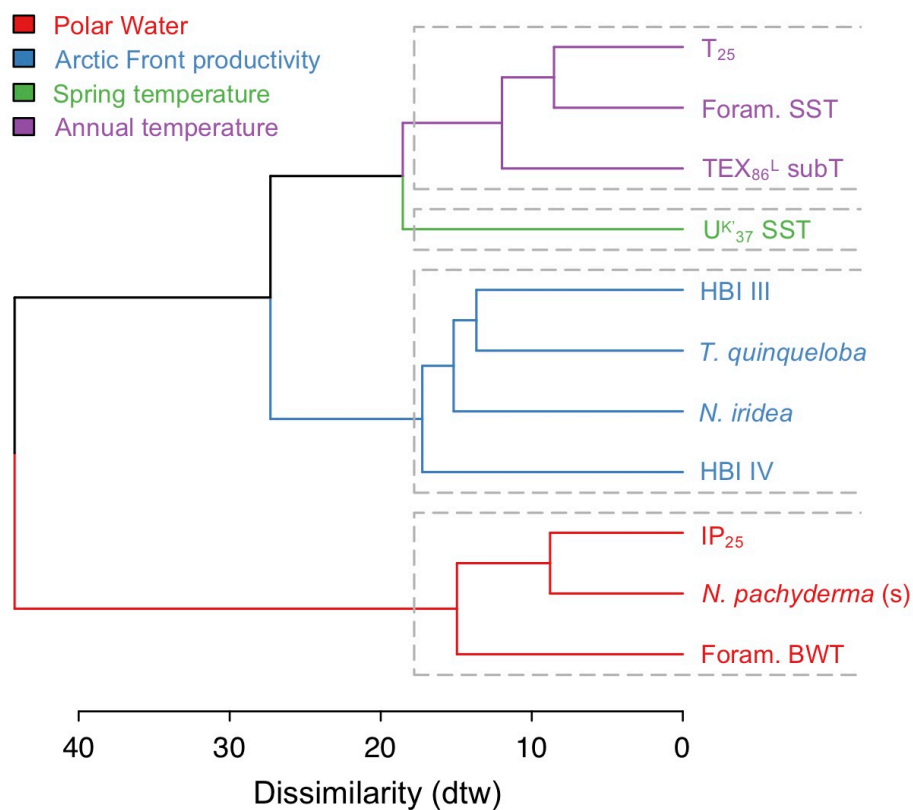
Figure 5: Four hierarchical clusters of select MD99-2269 productivity and temperature proxy records as determined by Dynamic Time Warping (DTW).
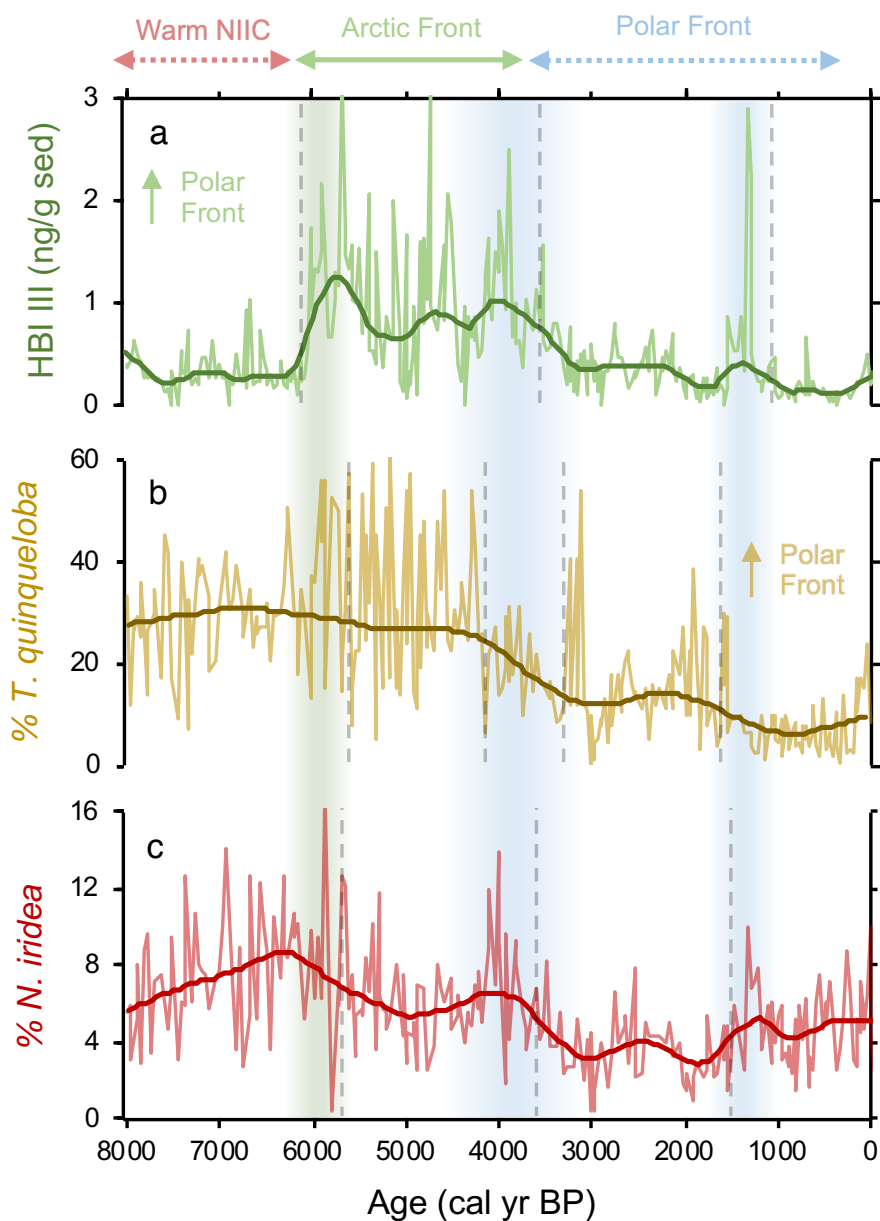
Fig. 6: Comparison between frontal proxies from marine sediment core MD99-2269. a) HBI III (Cabedo-Sanz et al., 2016), b) % *T. quinqueloba* planktic foraminifera, and c) % *N. iridea* benthic foraminifera. Vertical green bar indicates the timing of Polar Front establishment in the early Middle Holocene. The Middle Holocene blue bar indicates the southward migration and departure of the Polar Front from this location, and the Late Holocene blue bar indicates a period of further cooling interpreted from the proxy RSI values.

740
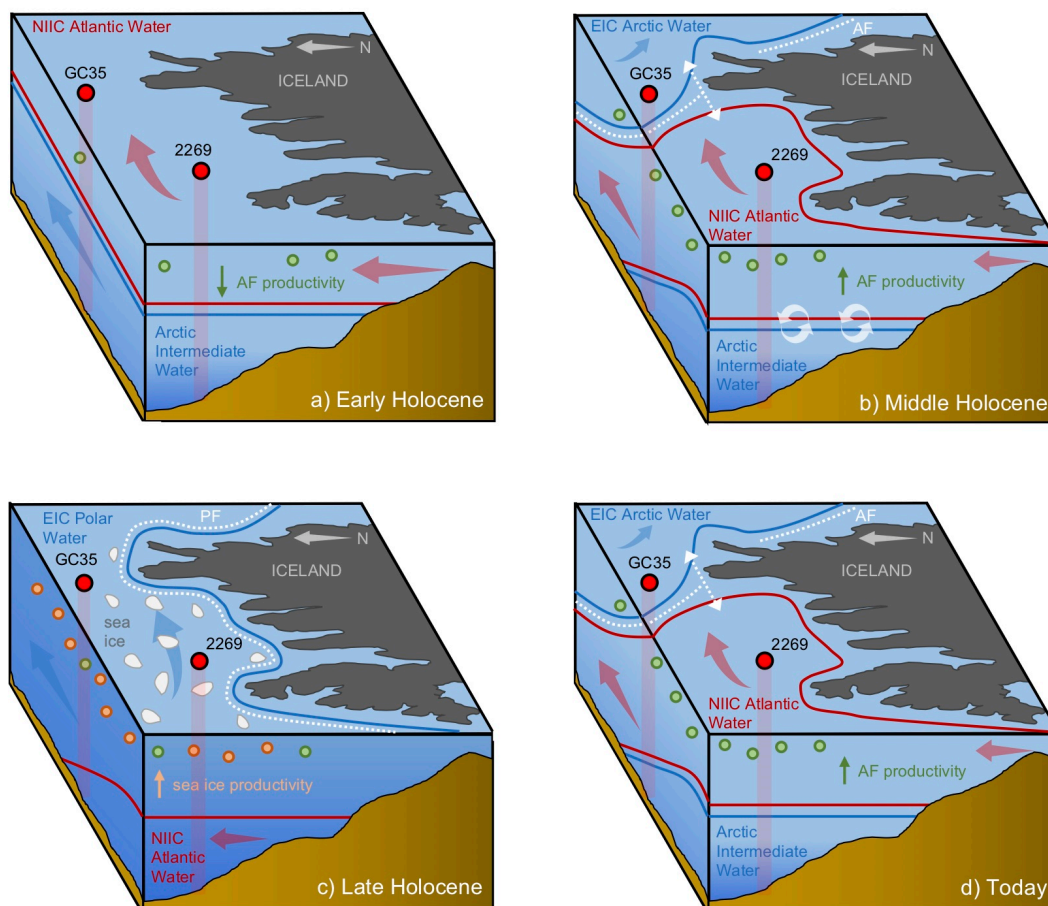
745

Figure 7: Schematic illustration of NIS oceanography and migration of the Arctic (AF) and Polar Fronts (PF) at four Holocene time slices. a) Early Holocene, where the NIS is characterized by NIIC Atlantic Water at the surface with the AF and PF north of both core sites. b) Middle Holocene migration of AF to the NIS and submergence of NIIC Atlantic Water beneath EIC Arctic Water on the east NIS. c) Late Holocene migration of the PF to the NIS with EIC Arctic/Polar Water present throughout the surface and above NIIC Atlantic Water. d) Today, where the AF is present on the NIS with NIIC Atlantic Water to the west and EIC Arctic Water to the east. Also shown are simplified direction of ocean currents (blue and red arrows), open water and sea ice productivity indicators (green and orange circles, respectively), and marine sediment core locations and profiles (red circles and columns) with abbreviated core names (i.e. MD99-2269=2269 and JR51-GC35=GC35).

755